

## Article

# The Influence of Biowaste Type on the Physicochemical and Sorptive Characteristics of Corresponding Biochar Used as Sustainable Sorbent

Nikolaos Mourgkogiannis, Ioannis Nikolopoulos , Eleana Kordouli , Alexis Lycourghiotis, Christos Kordulis  and Hrisi K. Karapanagioti 

Department of Chemistry, University of Patras, GR-26504 Patras, Greece; nikosmorgan@hotmail.com (N.M.); gs.nikol@gmail.com (I.N.); alycour@upatras.gr (A.L.); kordulis@upatras.gr (C.K.)

\* Correspondence: ekordouli@upatras.gr (E.K.); karapanagioti@upatras.gr (H.K.K.)

**Abstract:** Biowaste raw materials were used for biochar preparation through pyrolysis at 850 °C under a limited oxygen atmosphere. Raw materials and the corresponding biochar samples were characterized by XRD, FTIR, SEM, TGA, N<sub>2</sub>-sorption, pH-equilibrium, and ash content measurements. These samples were evaluated as sustainable sorbents for use in methylene blue (MB) removal from artificial fresh water. All biochar samples exhibited high specific surface areas (367–870 m<sup>2</sup>·g<sup>-1</sup>), low crystallinity, and low population of functional groups (C–O–C, –COOH, –N–O, –N–H, and –OH) on their surfaces. They were mainly micro-porous materials with a significant fraction of pores in the meso-porous range. The specific surface area of the latter pores proved very important for the physical adsorption of MB from aqueous solution. Although the raw materials exhibited low MB sorption capacity, ranging from 29 to 54 mg·g<sup>-1</sup>, the corresponding biochar samples exhibited important MB sorption efficiency ranging from 58 to 370 mg·g<sup>-1</sup>. Among the biochar samples studied, those produced from coffee residues proved most promising for MB removal from water solution (sorption capacity: 280–370 mg·g<sup>-1</sup>), addressing the United Nations Sustainability Development Goal (SDG) 6: Clean Water and Sanitation by improving the index related to anthropogenic wastewater that has received treatment.

**Keywords:** agricultural wastes; biowaste valorization; biochar; porous materials; pyrolysis; sustainable sorbent



**Citation:** Mourgkogiannis, N.; Nikolopoulos, I.; Kordouli, E.; Lycourghiotis, A.; Kordulis, C.; Karapanagioti, H.K. The Influence of Biowaste Type on the Physicochemical and Sorptive Characteristics of Corresponding Biochar Used as Sustainable Sorbent. *Sustainability* **2024**, *16*, 2889. <https://doi.org/10.3390/su16072889>

Academic Editor: Antoni Sánchez

Received: 28 February 2024

Revised: 26 March 2024

Accepted: 27 March 2024

Published: 30 March 2024



**Copyright:** © 2024 by the authors. Licensee MDPI, Basel, Switzerland. This article is an open access article distributed under the terms and conditions of the Creative Commons Attribution (CC BY) license (<https://creativecommons.org/licenses/by/4.0/>).

## 1. Introduction

The use of biomass as a natural resource to produce carbonaceous materials under thermal conditions contributes to long-term environmental protection by purifying aqueous systems and reducing CO<sub>2</sub> emissions while favoring sustainability. Biochar is a valuable product obtained from biomass heated under different pyrolytic conditions [1]. Pyrolysis is a thermal process through which organic substances decompose under a limited or very low oxygen atmosphere at a temperature range of 300 to 1300 °C. Biochar can be incorporated into soil as a soil amendment [2], providing organic matter amounts which prevent the physical breakdown of soil [3].

Past studies have shown that biochar obtained at high temperatures (750–900 °C) presents higher surface area and porosity compared to that produced at lower temperatures (300–600 °C) [4]. Another study also demonstrated that biochar yield decreases with increasing pyrolysis temperature [5]. Rasa et al. showed that pyrolysis temperature is a vital parameter affecting produced biochar [6]. Besides the pyrolysis temperature, the biomass type is another factor that determines the production of biochar with desirable properties. The lignin, cellulose, and hemicellulose contents of biomass used for biochar production affect the structure of the final product, whereas inorganic components result in biochar with high ash content and low volatile matter [7]. Both the chemical composition

and the physical properties, such as pore size, surface area etc., of biochar depend on the production conditions, such as pyrolysis temperature, atmosphere, and time, along with the feedstock characteristics [8]. Therefore, the use of suitable raw materials and pyrolysis conditions are essential for the production of high performance and low-cost biochar [9,10]. This environmentally friendly material shows great potential as a pollutants (heavy metals, dyes, etc.) sorbent for use in the purification of water. The advantages of biochar for use in place of other materials, such as activated carbon and inorganic sorbents, in the efficient removal of toxic heavy metals from aqueous systems has been extensively reviewed by Shakoor et al. [10].

Coffee is a widespread product and the most famous beverage around the world [11]. In 2021, coffee exports increased by 0.11 million bags compared to 2020 and reached 11.4 million unit [12]. Spent coffee grounds contain several classes of compounds, with polysaccharides comprising 50% of the total mass [13]. Greek coffee is a strongly brewed coffee that is found everywhere in Greece. It is similar to the coffee served in surrounding countries in the Middle East and is an integral part of the country's culture. Greek coffee is served with grounds in the cup. The grounds are allowed to settle as the coffee is slowly sipped. Therefore, large amounts of Greek coffee sediments end up in sewers without any form of treatment. Greek coffee contains large amounts of organic compounds [14]. Coffee sediments are a widely known pollutant and are hardly treated by conventional municipal wastewater treatment plants due to the fragmentary treatment of caffeine by microorganisms developed in these facilities [15].

Grapes are one of the most popular fruits worldwide. Approximately 75 million tons are produced every year, and 35 million tons are used to produce wine [16,17]. Grape seeds are considered a major winery waste product, comprising approximately 17% of the grape pomace mass [18]. In Greece, in 2021, approximately 695.6 thousand tons of grapes were produced [19], which corresponds to approximately 14 thousand tons of grape seeds in an annual base. These quantities render grape seeds among the popular biowastes found in Greece. Thus, the thermal degradation of grape seeds at elevated temperatures under oxygen-limited conditions seems to be a promising treatment for producing biochar with complex matrices. Grape seeds, after wine production, are also used to produce tsipouro, a Greek national distillate drink. Commercial tsipouro contains alcohol lower than 50% volume after water dilution [20]. Over the last decade, the tsipouro market has increased in size rapidly, producing 18.5 million L in 2012 (IWSR) in Greece. Seeds are the main waste product, among others (e.g., marcs), that should be treated after tsipouro production. However, several studies have shown that tsipouro contains many volatile compounds at significant concentrations [21]; hence, the thermal treatment of seeds remaining after tsipouro production is an issue that could be further explored.

Rice constitutes one of the largest crops in the world, with more than 500 million tons being produced every year. In Greece, the annual national rice harvest is estimated at 0.024% of the global rice production (approximately 120 thousand tons per year). Considering that rice husk represents 20% of the total amount of the grain produced [22], the annual production of rice husk in Greece is estimated approximately at 24 thousand tons per year. Hence, rice husk is an abundant biowaste which can be easily found in the Greek countryside. The high concentration of SiO<sub>2</sub> in rice husk compared to other biowastes, with SiO<sub>2</sub> comprising 96% of the inorganic compound content in the organic matrix of rice, makes it a favorable feedstock for the production of promising and cost-effective materials such as silica gel [23].

Although the aforementioned biowastes are not toxic, their management is not particularly environmentally friendly. While several extensive articles have reported on the physical and chemical characteristics of biochar obtained from spent coffee grounds [24,25] and rice husk [26], limited literature is available on the physicochemical characteristics of biochar derived from Greek coffee sediment, grape seeds after wine production, and grape seeds after distillation for tsipouro production.

From the above, it is obvious that biochar sorbents produced from biowastes satisfy the principles of circular economy concept, resulting in useful low-cost materials with significant environmental applications. The aim of the current study was to investigate the influence of various types of biowaste on biochar physicochemical and sorptive characteristics in a water purification context. Biochar samples obtained from five biowaste materials, processed via pyrolysis under a limited oxygen atmosphere, were studied. These biowastes, besides their different origin, also underwent different treatments. Rice husk and grape seeds for wine production underwent only mechanical treatment, Greek coffee sediment and grape seeds from tsipouro production underwent strong boiling, and espresso coffee grounds underwent instant contact with hot water. The main objectives of this study are: (a) evaluation of the biochar yield from each raw material, (b) comparison of the physicochemical properties of the different raw materials and biochar samples produced, and (c) investigation of the methylene blue (MB) sorption capability of the studied materials. MB was selected as a probe water pollutant representing cationic dyes found in the effluents of textile industries.

This study aims to increase sustainability and targets different United Nations Sustainability Development Goals (SDGs). It will positively affect SDG 6: Clean Water and Sanitation by improving the index related to anthropogenic wastewater that receives treatment. It also targets SDG 16: Life on Land by sustainably using terrestrial ecosystems, and not for disposing biowaste. SDG13: Climate Action is also targeted, specifically through not allowing the production of CO<sub>2</sub> emissions resulting from the degradation of biowaste in disposal sites.

## 2. Materials and Methods

*Material production.* Spent coffee grounds (SCG) and sediment from Greek coffee (SGC) were obtained from a coffee shop located on the campus of the University of Patras, Greece. Grape seeds after wine production (GSW) were obtained from Patraiki winery, Patras, Greece. Grape seeds after distillation for tsipouro production (GST) were obtained from a local distillery in the region of Patras, Greece, and rice husk (RH) was sourced from Agrino Company, Agrinio, Greece. The raw materials were oven dried in a Memmet oven at 50 °C for several hours until the moisture was removed and the constant weight of the solid was obtained. The method for biochar production was based on Manariotis et al. [4]. Dried samples were weighed and placed in a custom-made ceramic sagger box, closed with a cap to prevent oxygen from entering the vessel, and pyrolyzed at 850 °C for 1 h in a large electric furnace with a heating range of 30–3000 °C (Type Nabertherm, Controller B 180, Lilienthal, Germany). The pyrolysis temperature of 850 °C for biochar production using several forms of biowaste was chosen according to previous studies [4] to achieve the highest specific surface area (SSA) of biochar. Produced biochar was weighed and yield was calculated according to Equation (1):

$$\text{Biochar yield (\%)} = (\text{mass of biochar} / \text{mass of dry raw material}) \times 100\% \quad (1)$$

*Ash content.* The measurement of ash content was conducted using a standard method based on the findings of Kalaitzidis et al. [27]. For each of the examined samples, 1 g of sample was taken into a pre-calcined crucible for calcination at 750 °C in a furnace for 2 h. The crucible was then cooled to room temperature and reweighed. The ash content was calculated based on the Equation (2):

$$\text{ash (\%)} = (\text{mass of ash (g)} / \text{dry mass of sample (g)}) \times 100\% \quad (2)$$

To check the reproducibility of the results, duplicate samples were run.

*X-ray diffractions (XRD) analysis.* X-ray diffraction examination was performed on the materials studied, and the corresponding patterns were recorded in a 2θ range of 5–70° using a Bucker D8 Advance Diffractometer equipped with a nickel-filtered Cu Kα (1.5418 Å)

radiation source. XRD analysis was performed to investigate any possible crystal phase in the materials.

*Thermo-gravimetric analysis (TGA).* A thermo-gravimetric analyzer was used to reveal the weight loss characteristics of biochar. For each material, 7 mg of powdered sample was heated at a heating rate of  $20\text{ }^{\circ}\text{C}\cdot\text{min}^{-1}$  from room temperature to  $1000\text{ }^{\circ}\text{C}$  in a Perkin Elmer, Diamond TGA/DTA instrument. To check the reproducibility of the results, duplicate samples were run.

*SEM analysis.* Morphology visualization, along with the elemental composition of samples, were examined at different magnifications with a JEOL 6300 (SEMJEOL JSM6300, Tokyo, Japan) equipped with an X-ray energy dispersive spectrometer accessory. Photomicrographs were taken in the range of 1.36 to 27.08 K X magnification.

*Surface area and porosity.* The determination of the specific surface area (SSA), the external surface area, the pore volume, the micropore volume, and the average pore size for each sample was performed using  $\text{N}_2$  adsorption–desorption isotherms recorded in a Micromeritics TriStar 3000 Analyzer system. Before analysis, the raw materials were degassed at  $60\text{ }^{\circ}\text{C}$  under mild nitrogen flow for 2 h, and biochar was degassed at  $300\text{ }^{\circ}\text{C}$  under mild nitrogen flow for 1 h.

*Suspension  $\text{pH}_{\text{eq}}$ .* The suspension pH ( $\text{pH}_{\text{eq}}$ ) of raw materials and produced biochar samples was measured according to Manariotis et al. [4]. Approximately 20 mL of an electrolyte solution containing 0.1 M  $\text{NaNO}_3$  ( $\text{pH} = 7.0$ ) and 0.32 g of each sample were placed in 40 mL glass bottles. The suspension pH of the supernatant was measured after 24 h using a portable multi-parameter pH-meter (Consort C862) equipped with a glass electrode. To calibrate the glass electrode, two different pH buffer solutions, with pH equal to  $7.00 \pm 0.02$  and  $4.00 \pm 0.02$  at  $25\text{ }^{\circ}\text{C}$ , were used.

*Functional group analysis.* The chemical characteristics of the raw materials and produced biochar were identified using a PerkinElmer FTIR spectrometer. Approximately 0.5 mg of dried sample and 50 mg of dried KBr were mixed and turned into a pellet. The wavenumber measurement range was  $4000\text{--}400\text{ cm}^{-1}$  and was analyzed by IRSearchMaster 6.0 software.

*Sorption tests.* Methylene blue (MB) solutions were prepared in synthetic freshwater based on Karapanagioti et al. [28]. Approximately  $44\text{ mg}\cdot\text{L}^{-1}$  of  $\text{CaCl}_2\cdot 2\text{H}_2\text{O}$ ,  $14\text{ mg}\cdot\text{L}^{-1}$  of  $\text{CaSO}_4$ , and  $17\text{ mg}\cdot\text{L}^{-1}$  of  $\text{NaHCO}_3$  were added to 4 L of deionized water to adjust the ionic strength and salinity of the solution. MB adsorption experiments were carried out in 40 mL glass vials. A stock solution of  $20\text{ mg}\cdot\text{L}^{-1}$  of MB was prepared in synthetic freshwater. About 3 mg of each sorbent (raw materials and biochar samples produced) were placed into the glass vials, and MB stock solution was added. Blanks were also prepared containing only the MB stock solution without sorbent. For all samples, measurements of the aqueous concentration were taken after 24 h and at various time periods up to 137 days for some samples. All samples and blanks were prepared in triplicates.

Aqueous MB concentration was determined by a HACH DR/2400 portable spectrophotometer (Loveland, CO, USA), using a cuvette of 1 cm at 670 nm. The amounts of MB sorption for the tested samples were calculated by Equation (3):

$$q_t = \frac{(C_o - C_t) \times V}{m} \quad (3)$$

where  $q_t$  ( $\text{mg}\cdot\text{g}^{-1}$ ) is the sorption capacity of the solid at sampling time  $t$ ,  $C_t$  ( $\text{mg}\cdot\text{L}^{-1}$ ) is the aqueous concentration of MB at sampling time  $t$ ,  $C_o$  ( $\text{mg}\cdot\text{L}^{-1}$ ) is the initial aqueous concentration of MB (determined by the blank sample to account for possible method MB losses), also measured at time  $t$ ,  $V$  (mL) is the volume of the MB stock solution used, and  $m$  (g) is the sorbent mass added in the vials of 40 mL.

In the current study, the MB adsorption kinetics were well described by a pseudo-first order Equation (4):

$$\frac{dq}{dt} = k_1 \times (q_e - q_t) \Rightarrow \ln(q_e - q_t) = \ln q_e - kt \quad (4)$$

where  $k_1$  is the constant of the pseudo-first-order rate ( $\text{min}^{-1}$ ),  $q_t$  is the amount of MB adsorbed per mass of sorbent at time  $t$  ( $\text{mg}\cdot\text{g}^{-1}$ ), and  $q_e$  is the amount of MB adsorbed per mass of sorbent at equilibrium ( $\text{mg}\cdot\text{g}^{-1}$ ).

### 3. Results and Discussion

#### 3.1. Material Moisture, Ash Content and Biochar Yield

The moisture contents of the raw samples, which were calculated by subtracting the mass after initial drying at 50 °C from that before drying, are listed in Table 1. The moisture contents ranged from 4 to 63%. The highest percentage of moisture was detected in the SCG sample (63%), while the GSW and GST samples showed approximately the same moisture percentage (20% and 18%, respectively). SGC had a moisture content of 11%, and rice husks had the lowest moisture content (4%).

**Table 1.** pH<sub>Eq</sub>, moisture and ash content, and different yields for biochar production at 850 °C.

Samples	pH <sub>Eq</sub>	Moisture Content of Raw Materials (%)	Yield of Initial Material in Biochar (%)	Yield of Dry Raw Material in Biochar (%)	Ash Content (%) *	Yield of Dry Raw Material in Carbonaceous Material Fraction in Biochar (%)
SCG	5.5	63	-	-	1.7	-
SCG-B	10.6	-	3.6	9.8	13 (17)	8.6
SGC	6.4	11	-	-	1.2	-
SGC-B	10.3	-	6.0	6.8	12 (18)	6.0
GSW	5.8	20	-	-	2.6	-
GSW-B	10.2	-	17	21	7 (10)	20
GST	7.0	18	-	-	2.4	-
GST-B	10.7	-	16	20	9 (15)	18
RH	6.0	4	-	-	18	-
RH-B	9.4	-	27	28	60 (64)	11

\* Values in parentheses are the predicted percentage of ash content in the biochar based on the raw material ash and the yield of the dry raw material in biochar.

Pyrolysis temperature and inorganic content are considered parameters which crucially affect biochar yield [29] and ash content [30,31]. Table 1 shows the percentages in mass yield of biochar obtained from the pyrolyzed dry materials. These range from 6.8 to 28%. The highest biochar yield was 28%, and corresponded to RH. The yield order for the studied biochar from the highest to the lowest value is: RH > GSW > GST > SCG > SGC. The yield of biochar is strongly interrelated both with the percentage of inorganic mater (ash) and the thermal degradation of cellulose, hemicellulose, and lignin found in the structure of the materials [32]. If the biochar yield is calculated on the basis of the initial raw biomass (before drying), it is less (3.6–27%), as expected, but there is not any linear correlation with the moisture content.

Yargiloglou et al. determined the physicochemical properties of biochar obtained from logging residues and found that an increase in ash content is strongly correlated with the presence of polycyclic aromatic hydrocarbons (PAHs) and metals detected in biochar [33]. The low ash content of biochar is related to the small amount of metals found in the carbonaceous materials [34,35]. Table 1 shows that, with the exception of RH, the raw materials used had relatively low ash content ( $\leq 13\%$ ). It is well known that RH contains a significant fraction of SiO<sub>2</sub>, explaining the high ash content (60%) determined (Table 1). Dawei et al. used a rice husk-based SiO<sub>2</sub>/C composite to increase the performance of lithium batteries and found that the treatment of this composite material with a high

concentration of alkaline solution (NaOH) led to a decrease in silica content, which was followed by a reduction in ash content of the tested sample [36]. It is obvious that the high pyrolysis temperature (850 °C), as well as the proportion of inorganic matter contained in each material, play a decisive role in the ash content of the biochar samples [30,31].

### 3.2. Material Structure

The XRD patterns of the raw materials studied, and the corresponding biochar products, are presented in Figure 1. In general, two wide peaks in the  $2\theta$  ranges at 20–30° and 35–45° (with exception of GSW, GST, and RH) were observed in the XRD patterns of raw materials, which is indicative of their cellulosic nature and low crystallinity [37]. In the XRD patterns of the biochar samples, these peaks were shifted towards slightly higher  $2\theta$  angle values, indicating the formation of a graphitic phase involving carbon species with  $sp^2$  hybridization [38,39].

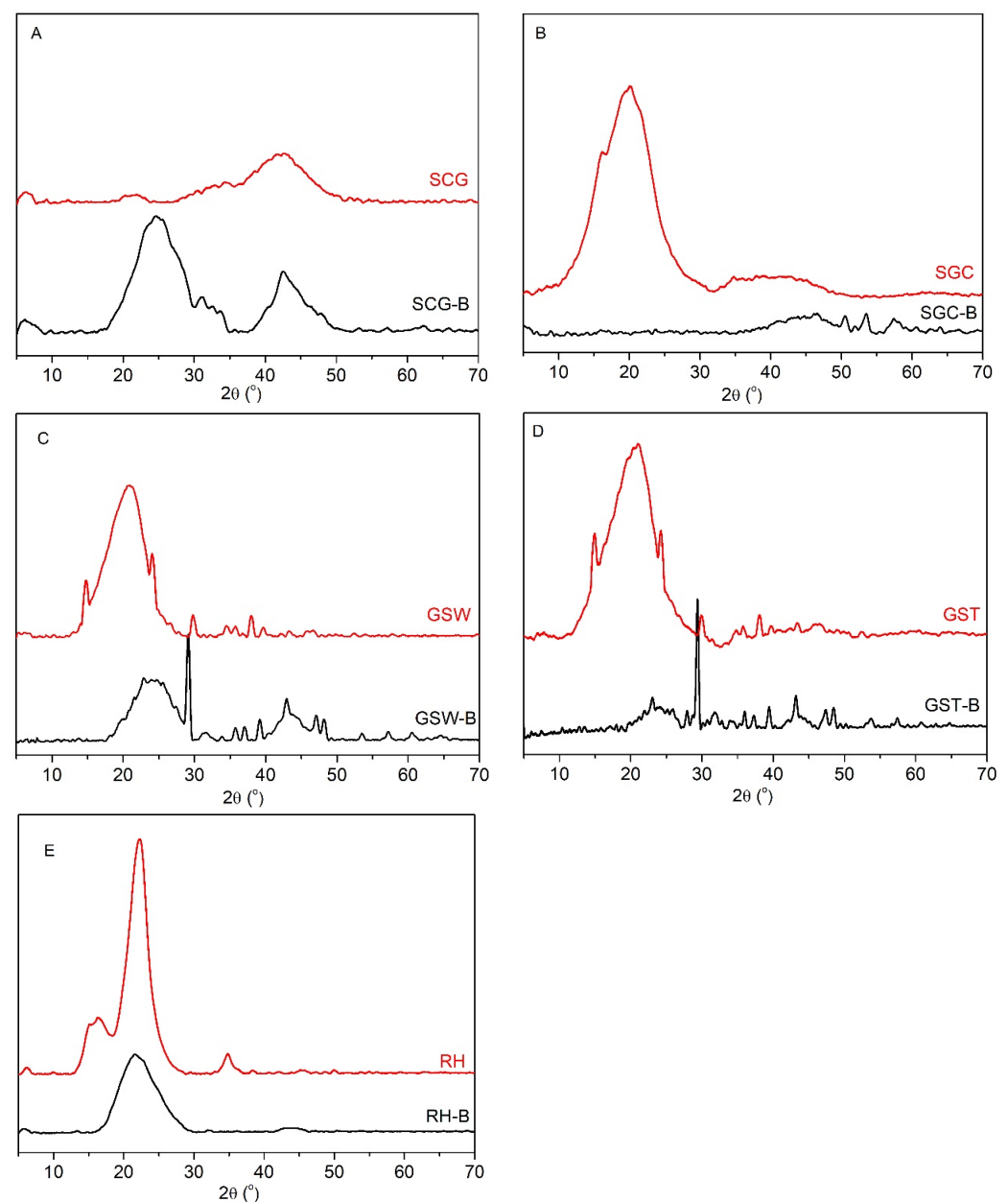


**Figure 1.** XRD patterns of the raw materials and the corresponding biochar samples studied; (A): SCG and SCG-B, (B): SGC and SGC-B, (C): GSW and GSW-B, (D): GST and GST-B and (E): RH and RH-B.

More precisely, Figure 1A indicates that the SCG is almost amorphous. The observed XRD peaks at around  $25^\circ$  and  $43^\circ$  in the SCG-B pattern indicates that the obtained biochar was a typical carbonaceous material with porous structure produced via the disintegration of lignin, cellulose, and hemicellulose. Figure 1B shows that biochar produced through the pyrolysis of SGC is a completely amorphous material. Figure 1C,D show that the biochar produced via pyrolysis of grape seeds exhibited the characteristic XRD patterns of biochar with lignocellulosic origin. An inspection of these patterns revealed that additional sharp peaks appeared at  $2\theta$ :  $\sim 30^\circ$  (strong),  $36^\circ$ ,  $39.4^\circ$ , and  $43.1^\circ$ , which correspond to calcite ( $\text{CaCO}_3$ ) crystallites [40] and could be related to strong bonding between condensed carbon with Ca salts or  $\text{SiO}_4$  [41]. This is in agreement with the elemental analysis (EDS) of the GSW-B and GST-B samples, indicating the existence of Ca and Si in them (Table S1). Figure 1E shows that the XRD pattern of RH presented peaks at  $12^\circ$ ,  $15^\circ$ , and  $21^\circ$ , revealing the presence of crystalline cellulose and some five carbon sugars [42]. The XRD pattern of pyrolyzed RH (RH-B) was quite different, exhibiting a broad peak in the  $2\theta$  range  $20\text{--}30^\circ$ , which is characteristic of biochar of lignocellulosic origin. This peak was deconvoluted into two peaks centered at  $20^\circ$  and  $25^\circ$ ; the first one was attributed to the  $\text{SiO}_2$  contained in RH-B [43], and the second to the carbonaceous material in biochar.

### 3.3. Raw Materials Pyrolysis and Thermal Stability of Biochar

The results of the thermogravimetric (TG) analyses of raw materials used for biochar production are presented in Figure 2A. In all cases, raw materials lost mass at two distinct temperature ranges. At low temperatures ( $<200^\circ\text{C}$ ), the mass loss was attributed to the removal of moisture and volatile compounds. A dramatic mass loss was observed in the range  $350\text{--}500^\circ\text{C}$  and was attributed to the degradation/pyrolysis of lignocellulosic matter, followed by a slight mass loss up to  $1000^\circ\text{C}$  due to further degradation [8]. An inspection of Figure 2A shows that the mass loss upon TG analysis of raw materials increased in the following order:  $\text{SGC} > \text{SCG} > \text{GST} > \text{GSW} > \text{RH}$ . As is expected [44], this order is the inverse of that based on the ash content of the raw materials (Table 1), indicating that mass loss was mainly determined by the pyrolysis of the organic fractions of raw materials.

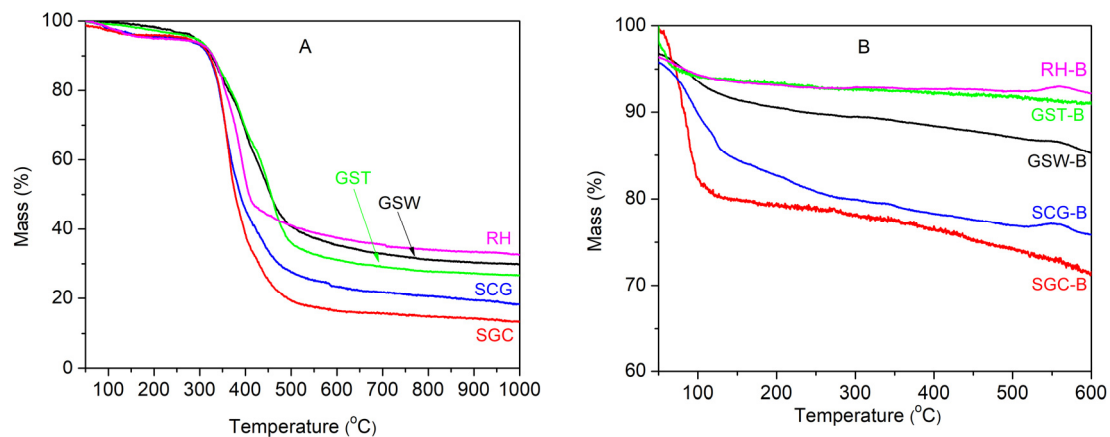


**Figure 2.** Thermogravimetric analysis of the raw materials (A) and the corresponding biochar samples (B).

TG analysis of biochar samples produced revealed that a significant mass loss took place at low temperatures (lower than  $\sim 250^\circ\text{C}$ ), while mass declined slightly at higher temperatures (Figure 2B). The initial mass loss observed can be attributed to the removal of the moisture that was adsorbed on the biochar surface upon their storage. This agrees with the fact that the mass loss of biochar in the aforementioned area follows the same trend as that followed by their SSA and pore volume (see Table 2). The relevant stability of the samples at higher temperatures (up to  $600^\circ\text{C}$ ) was expected because of their thermal pretreatment (pyrolysis) at even higher temperatures ( $850^\circ\text{C}$ ).

**Table 2.** Biochar textural characteristics (SSA: specific surface area,  $SSA_{Micro}$ : t-plot micropore area,  $SSA_{External}$ : t-plot external surface area, SPV: specific pore volume,  $SPV_{Micro}$ : t-plot micropore volume, and MPD: mean pore diameter).

Biochar	SSA ( $m^2 \cdot g^{-1}$ )	$SSA_{Micro}$ ( $m^2 \cdot g^{-1}$ )	$SSA_{External}$ ( $m^2 \cdot g^{-1}$ )	SPV ( $cm^3 \cdot g^{-1}$ )	$SPV_{Micro}$ ( $cm^3 \cdot g^{-1}$ )	MPD (nm)
SCG-B	751	514	237	0.39	0.24	3.1
SGC-B	870	587	283	0.44	0.27	3.1
GSW-B	529	420	109	0.27	0.19	3.8
GST-B	464	350	114	0.24	0.17	3.8
RH-B	367	230	137	0.23	0.11	4.3

### 3.4. Chemical Characteristics

Figure 3 shows the FTIR spectra of raw materials and the corresponding biochar samples. The raw materials spectra present several peaks assigned to various functional groups.

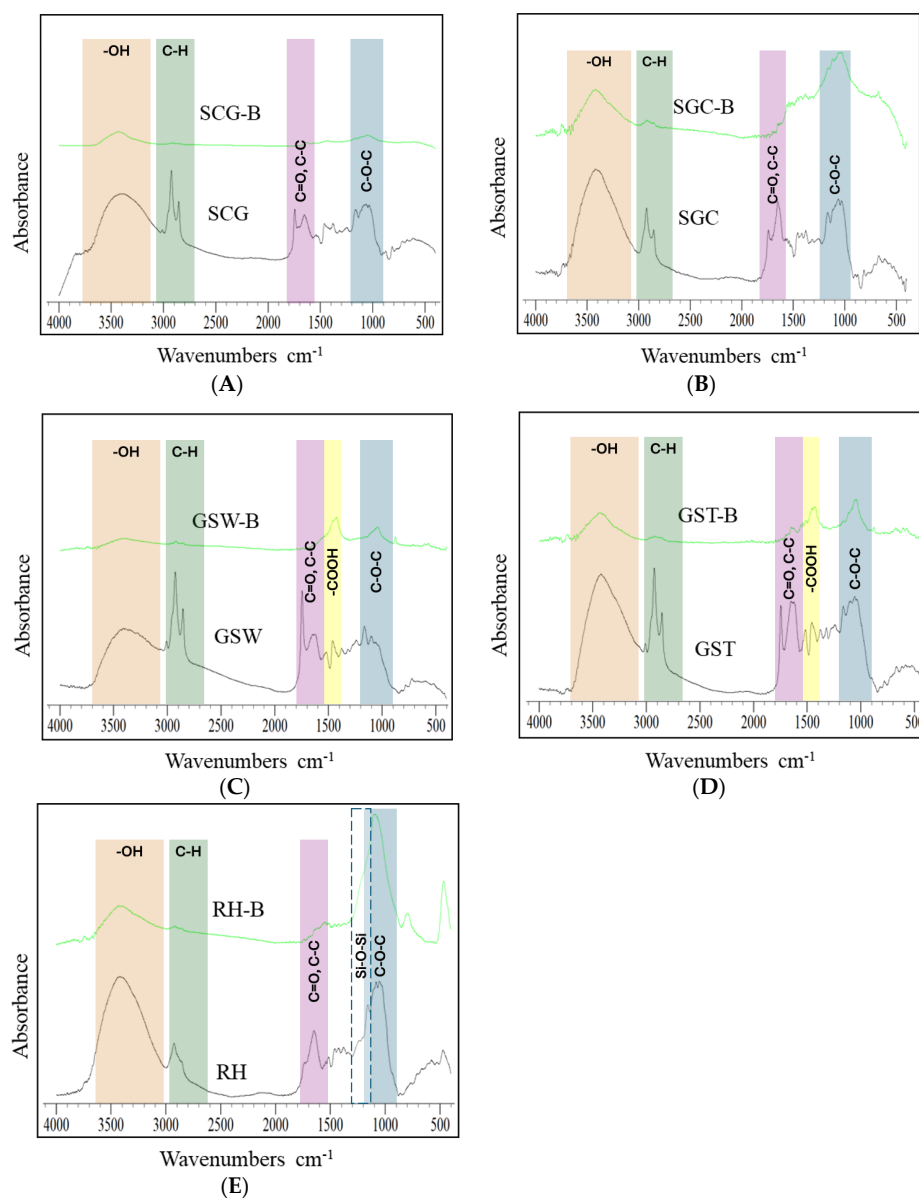


**Figure 3.** FTIR spectra of raw materials and corresponding biochar samples studied; (A): SCG and SCG-B, (B): SGC and SGC-B, (C): GSW and GSW-B, (D): GST and GST-B and (E): RH and RH-B.

The peaks between 3400 and 3600  $\text{cm}^{-1}$  indicated the presence of  $-\text{OH}$  groups on both raw materials and biochar. The raw materials spectra presented peaks at 2855 and 2920  $\text{cm}^{-1}$  that corresponded to aliphatic  $\text{C}-\text{H}$  stretching, attributed to the hemicellulose and cellulose components. Peaks appearing near 1740  $\text{cm}^{-1}$  were attributed to  $\text{C}=\text{O}$  stretching vibration, indicating the existence of esters, carboxylic acids, and ketones [45], while peaks at 1590–1650  $\text{cm}^{-1}$  were assigned to aromatic  $\text{C}=\text{O}$  and  $\text{C}-\text{C}$  stretching associated with the lignin fraction of raw materials [46]. Peaks appearing in the region 900–1200  $\text{cm}^{-1}$  were considered characteristics of  $\text{C}-\text{O}-\text{C}$  and  $\text{C}-\text{O}$  ring vibrations in various polysaccharides [47].

The aforementioned peaks either decreased or totally vanished in the corresponding biochar spectra [48]. Fu et al. studied the FTIR spectra of biochar samples produced at temperatures higher than 600  $^{\circ}\text{C}$  and claimed that the adsorption bands recorded indicated the existence of mainly aromatic and ether structures [49].

The FTIR spectra of the biochar samples studied were quite similar. An absorbance peak in the range 1000–1100  $\text{cm}^{-1}$ , which predominated in all spectra, was attributed to  $\text{C}-\text{O}-\text{C}$  stretching vibration [48]. The highest intensity of this peak was observed in the FTIR spectrum of the RH-B sample. In this case, an overlap of the aforementioned absorption with the asymmetric  $\text{Si}-\text{O}-\text{Si}$  stretching could have taken place due to the high silica content of RH [50]. Absorbance peaks in the ranges 1400–1500, 1500–1550, 1580–1650, and 3200–3600  $\text{cm}^{-1}$  were assigned to the presence of  $-\text{COOH}$ ,  $-\text{N}-\text{O}$ ,  $-\text{N}-\text{H}$ , and  $-\text{OH}$  groups, respectively [51].

### 3.5. Morphology of the Samples

Figure S1 presents the obtained SEM micrographs of the raw materials and biochar samples. These micrographs show that upon pyrolysis at 850  $^{\circ}\text{C}$ , the relatively smooth surface of raw materials was transformed and became rough due to pore formation. Table S1 presents the EDS semi-quantitative elemental analysis of the materials studied. As was expected, in all cases, C and O were the predominant elements. Ca, Mg, K, and Si existed as elements in most of the samples, while Na and Al were detected in the GST-B sample. Pyrolysis provoked a decrease in the oxygen content, thus increasing the weight percentage of the remaining elements.

### 3.6. Biochar Surface Area and Porosity

$\text{N}_2$  adsorption-desorption isotherms recorded at liquid nitrogen temperature were used to study the texture of the raw materials and biochar samples obtained (Figure S2).

Table 2 displays the values for the textural characteristics of biochar samples. Although the raw materials used had very low SSAs ( $<0.53 \text{ m}^2 \cdot \text{g}^{-1}$ ) and almost no pores (Figure S1), their pyrolysis for 1 h at 850  $^{\circ}\text{C}$  resulted in biochar samples with high total SSAs (367–870  $\text{m}^2 \cdot \text{g}^{-1}$ ). The t-plot analysis of  $\text{N}_2$  adsorption data revealed that the main part of their surface was inside of micro-pores (pore diameter lower than 2 nm,  $\text{SSA}_{\text{Micro}}$ ), representing percentage values in the range of 62–78% of SSA. Similarly, the specific volume of micro-pores corresponded to 47–71% of the specific pore volume. The mean pore diameter of biochar samples was in the range of 3.1–4.3 nm.

A more detailed picture of pore size can be obtained by inspecting Figure 4, which shows the pore size distribution curves of the biochar samples studied. It is obvious that all biochar samples were mainly microporous materials, especially those produced from coffee residues (SGC-B and SCG-B).

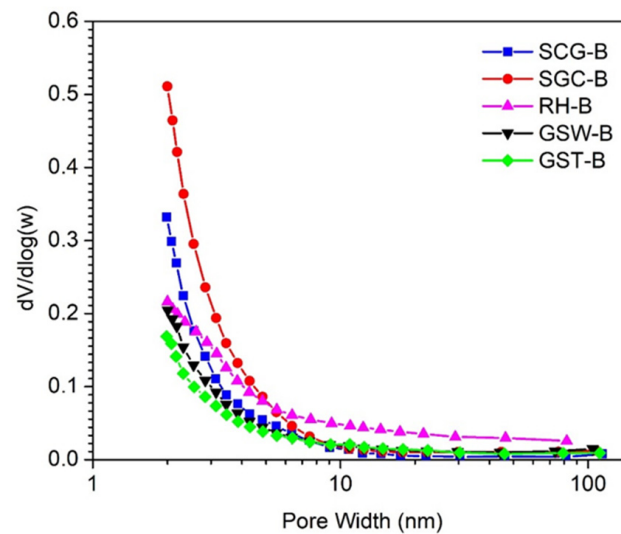


**Figure 4.** Pore size distribution curves of the biochar samples studied.

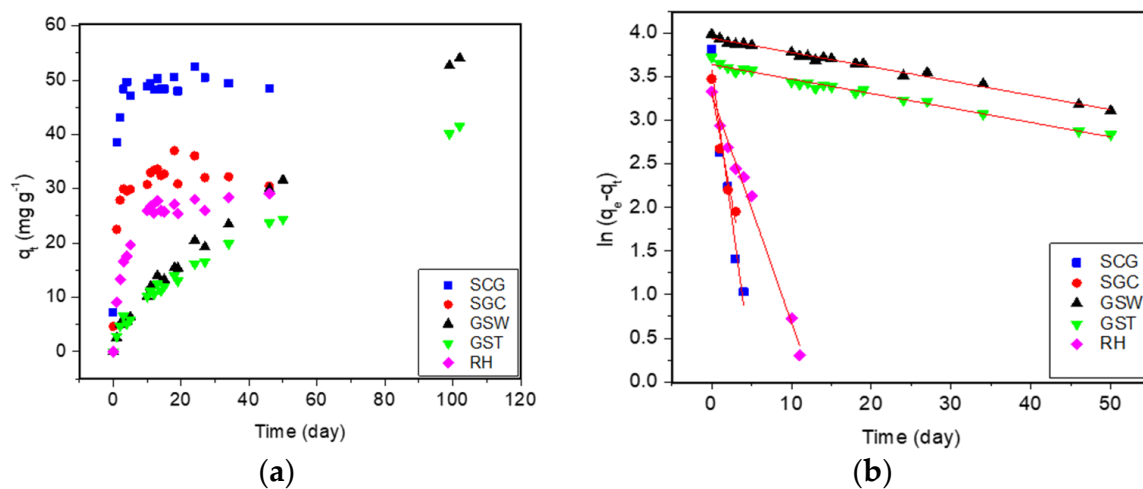
It is well known that the volatile matter of biomass is removed during the pyrolysis procedure, creating pores that increase thus the surface area of the biochar [52]. In addition, the destruction (dehydration and deoxygenation) of the carbohydrate, aromatic, and phenolic components of biomass causes a further increase in the porosity and SSA of the obtained biochar [53]. Manariotis et al. reported that the SSA of biochar obtained from malt spent rootlets at a high pyrolysis temperature gradually increased according to the development of a microporous structure [4]. Bonelli et al. stated that the pyrolysis of Brazil shell nuts at a high temperature produced biochar with high SSA, and as the temperature increased, micropores came to comprise most of the pore volume [54].

### 3.7. Suspension $pH_{eq}$

The  $pH_{eq}$  values for the raw materials suspensions were in the range 5.5–7.0 and shifted to higher values for the produced biochar samples (Table 1). The high biochar  $pH_{eq}$  values are concomitant with the biochar ash content, and could be explained by the volatilization of the  $-COOH$  and  $-OH$  functional groups and the simultaneous condensation of alkali and alkaline macronutrient (Na, Mg, K, Ca) salts or oxides that took place upon pyrolysis [55]. It should be stressed that the high  $pH_{eq}$  values (9.4–10.7) of biochar are not favorable for the electrostatic adsorption of cationic MB.

### 3.8. Methylene Blue Sorption

Figure 5a shows the MB sorption data collected using the raw materials as sorbents. Inspection of this figure indicates that SCG, SGC, and RH reached their equilibrium sorption capacity in less than 10 days. In contrast, grape seeds (SGW and SGT) did not reach an equilibrium plateau, even after 102 days. This slow sorption of MB observed in the latter materials could be attributed to their small external area and significantly greater mean particle size (~2.5 mm) in comparison with the remainder of the raw materials (<0.5 mm). However, in all cases, the sorption efficiency of the raw materials studied was low (<60  $mg \cdot g^{-1}$ ). This finding could be easily correlated with the low SSA (<0.53  $m^2 \cdot g^{-1}$ ) of these materials. Figure 5b shows that in all cases, sorption kinetics could be described quite well by adopting a pseudo-first order kinetic model.



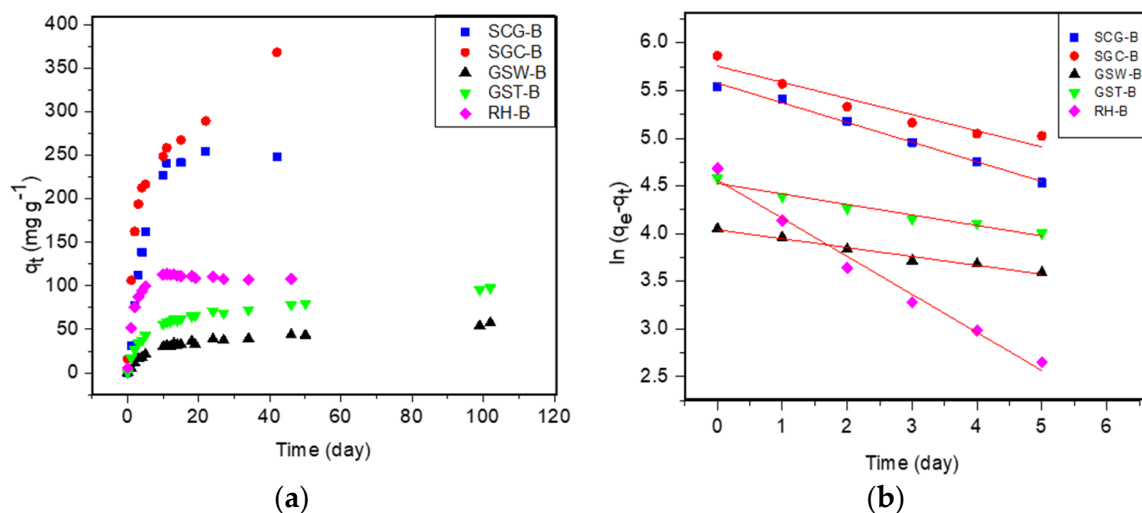
**Figure 5.** Variation of MB sorption in raw materials studied over time (a). Fitting of MB sorption kinetics on a pseudo-first order model (b).

Table 3 compiles the kinetic constant values calculated, the theoretical and experimental equilibrium sorption capacity values determined, and the  $R^2$  values of the straight lines fitted to the experimental data. The values of the latter parameter confirm the fairly good fit of the kinetic results to the pseudo-first order kinetic model. The  $k_1$  values calculated for the adsorption of MB on biochar samples produced from coffee residues are lower than those calculated using the corresponding raw materials as sorbents. This is not the case for the rest of the materials studied. One could attribute this different behavior to the low mean pore diameter (3.1 nm) of the first biochar samples, which probably retarded the MB mass transfer inside the pores. In contrast, the rest of the biochar samples exhibited higher mean pore diameters (3.8–4.1 nm), associated with lower mass transfer resistance, and thus higher  $k_1$  values, than those of the corresponding raw materials. The rate of MB sorption in grape seeds was very slow (0.02 day<sup>-1</sup>). However, these seeds exhibited final MB capacity values ( $q_{e \text{ exp final}}$ ) among the highest determined. This could be due to the slow absorption of MB inside the mass of the seeds.

**Table 3.** Experimental sorption capacity ( $q_{e \text{ exp}}$  and  $q_{e \text{ exp final}}$ ), theoretical adsorption capacity ( $q_e$ ), and kinetic constant ( $k_1$ ) for a pseudo first-order kinetic model, square of correlation coefficient ( $R^2$ ).

Experimental and Theoretical Sorption Parameters	Materials									
	SCG	SCG-B	SGC	SGC-B	GSW	GSW-B	GST	GST-B	RH	RH-B
$k_1$ (day <sup>-1</sup> )	0.68	0.21	0.50	0.17	0.02	0.09	0.02	0.11	0.26	0.39
$q_e$ (mg·g <sup>-1</sup> )	36	265	28	316	52	57	38	92	27	96
$q_{e \text{ exp}}$ (mg·g <sup>-1</sup> )	49	208	31	249	10	30	10	56	20	100
$q_{e \text{ exp final}}$ (mg·g <sup>-1</sup> )	53	280	35	370	54	58	42	99	29	110
$R^2$	0.952	0.995	0.914	0.905	0.989	0.976	0.982	0.952	0.990	0.980

Figure 6a shows the MB adsorption data on the surfaces of the biochar samples studied. All biochar samples reached adsorption plateau within the first ten days, except the SGC-B, for which sorption seemed to continue with a different slope.



**Figure 6.** Variation of MB sorption on biochar samples studied over time (a). Fitting of MB sorption kinetics on a pseudo-first order model (b).

Figure 6b reveals the good fitting of adsorption experimental data with the pseudo first-order kinetic model adopted. The slopes of corresponding straight lines were used for the calculation of adsorption rate constant values ( $k_1$ ).

Table 3 shows that, except for SGC-B, for the rest of biochar samples studied, the adsorption capacity values ( $q_e$ ) predicted by the pseudo first-order kinetic model were close to the values measured at the end of the corresponding test ( $q_{e \text{ final exp}}$ ). In the case of the SGC-B, the latter value measured was higher than predicted. This can be attributed to the high SSA ( $870 \text{ m}^2 \cdot \text{g}^{-1}$ ) of SGC-B, of which 67.5% was located in micro-pores (Table 2). This explains the slow second sorption step observed after the first ten days due to slow diffusion phenomena.

Summarizing the MB sorption efficiency of the materials tested in this study, it should be noted that: (i) the raw materials had low MB sorption capacity, ranging from 29 to  $54 \text{ mg} \cdot \text{g}^{-1}$ , and (ii) the biochar derived, with exception of GSW-B ( $58 \text{ mg} \cdot \text{g}^{-1}$ ), exhibited remarkable MB sorption efficiency, ranging from 99 to  $370 \text{ mg} \cdot \text{g}^{-1}$ . Similar values were reported as maximum sorption capacity ( $q_{\text{max}}$ ) in Orfanos et al. [56], which presented a summary of several references studying methylene blue sorption by biowaste ( $18\text{--}240 \text{ mg} \cdot \text{g}^{-1}$ ) and their corresponding biochar ( $127\text{--}132 \text{ mg} \cdot \text{g}^{-1}$ ). Table 3 shows also that the sorption efficiency trend followed by the biochar samples studied (SGC-B > SCG-B > RH-B > GST-B > GSW-B) is the same as that followed by their  $\text{SSA}_{\text{External}}$  values, presented in Table 2. Santoso et al., reviewing recent advances in carbon-based sorbents for MB removal from wastewater, have concluded that the removal efficiency is affected more by specific surface area than the pore size of sorbents [57]. This is expected, as the adsorption of MB in such materials is physical in nature [57]. However, our results showed that the surface area of pores with a diameter higher than  $\sim 2 \text{ nm}$  played the main role in the physical adsorption of MB by the samples.

#### 4. Conclusions

Biochar samples obtained via pyrolysis of biowaste (spent coffee grains, sediment of Greek coffee, grape seeds remaining after wine production, grape seeds remaining after tsipouro production, and rice husk) exhibit high specific surface areas, low crystallinity, and low population of functional groups. Although these biochar samples are mainly microporous materials, they have a significant fraction of pores in the meso-porous range. The specific surface area of the latter pores proved very important for the physical adsorption of methylene blue from aqueous solution. The raw materials with very low SSA had low MB sorption capacity, ranging from 29 to  $54 \text{ mg} \cdot \text{g}^{-1}$ , whereas the biochar samples, with exception of GSW-B ( $58 \text{ mg} \cdot \text{g}^{-1}$ ), exhibited remarkable MB sorption efficiency, ranging

from 99 to 370 mg·g<sup>-1</sup>. The sorption efficiency trend of the biochar samples is the same as that followed by their SSA<sub>External</sub> values (SGC-B > SCG-B > RH-B > GST-B > GSW-B). This study revealed that different biowastes can be transformed to biochar with interesting sorption properties, satisfying the principles of circular economy. Among the biochar samples studied, those produced from coffee residues proved very promising for MB removal from water solutions.

**Supplementary Materials:** The following supporting information can be downloaded at: <https://www.mdpi.com/article/10.3390/su16072889/s1>, Table S1: EDS elemental analysis of the materials studied; Figure S1: SEM micrographs of raw materials and biochar samples obtained. (a) SCG, (b) SCG-B, (c) SGC, (d) SGC-B, (e) GSW, (f) GSW-B, (g) GST, (h) GST-B, (i) RH, and (j) RH-B; Figure S2: N<sub>2</sub> adsorption-desorption isotherms recorded at liquid nitrogen temperature of raw materials and biochar samples obtained [58].

**Author Contributions:** Conceptualization, H.K.K., A.L. and C.K.; methodology, E.K.; software, N.M. and I.N.; validation, E.K., H.K.K. and C.K.; investigation, I.N., N.M. and E.K.; resources, C.K. and H.K.K.; data curation, E.K.; writing—original draft preparation, N.M.; writing—review and editing, E.K., C.K., A.L. and H.K.K.; visualization, E.K.; supervision, H.K.K.; project administration, E.K.; funding acquisition, C.K. All authors have read and agreed to the published version of the manuscript.

**Funding:** We acknowledge support of this work by the project “Research Infrastructure on Food Bioprocessing Development and Innovation Exploitation—Food Innovation RI” (MIS 5027222), which is implemented under the Action “Reinforcement of the Research and Innovation Infrastructure”, funded by the Operational Programme “Competitiveness, Entrepreneurship and Innovation” (NSRF 2014-2020) and co-financed by Greece and the European Union (European Regional Development Fund).

**Institutional Review Board Statement:** Not applicable.

**Informed Consent Statement:** Not applicable.

**Data Availability Statement:** All data supporting the reported results can be found in the published article.

**Acknowledgments:** We acknowledge the contribution of V. Dracopoulos (FORTH/ICE-HT) for recording SEM images and for the EDS mapping of the materials studied.

**Conflicts of Interest:** The authors declare no conflicts of interest.

## References

1. Lehmann, J.; Joseph, S. *Biochar for Environmental Management: Science, Technology and Implementation*, 2nd ed.; Lehmann, J., Joseph, S., Eds.; Routledge: London, UK, 2015; 976p. [CrossRef]
2. Chan, K.Y.; Van Zwieten, L.; Meszaros, I.; Downie, A.; Joseph, S. Agronomic values of greenwaste biochar as a soil amendment. *Aust. J. Soil Res.* **2007**, *45*, 629–634. [CrossRef]
3. Yang, B.; Li, D.; Yuan, S.; Jin, L. Role of biochar from corn straw in influencing crack propagation and evaporation in sodic soils. *CATENA* **2021**, *204*, 105457. [CrossRef]
4. Manariotis, I.D.; Fotopoulou, K.N.; Karapanagioti, H.K. Preparation and characterization of biochar sorbents produced from malt spent rootlets. *Ind. Eng. Chem. Res.* **2015**, *54*, 9577–9584. [CrossRef]
5. Demirbas, A. Effects of temperature and particle size on bio-char yield from pyrolysis of agricultural residues. *J. Anal. Appl. Pyrolysis* **2004**, *72*, 243–248. [CrossRef]
6. Rasa, K.; Viherä-Aarnio, A.; Rytönen, P.; Hyväluoma, J.; Kaseva, J.; Suhonen, H.; Jyske, T. Quantitative analysis of feedstock structural properties can help to produce willow biochar with homogenous pore system. *Ind. Crops Prod.* **2021**, *166*, 113475. [CrossRef]
7. Keiluweit, M.; Nico, P.S.; Johnson, M.G.; Kleber, M. Dynamic Molecular Structure of Plant Biomass-Derived Black Carbon (Biochar). *Environ. Sci. Technol.* **2010**, *44*, 1247–1253. [CrossRef] [PubMed]
8. Wang, S.; Gao, B.; Zimmerman, A.R.; Li, Y.; Ma, L.; Harris, W.G.; Migliaccio, K.W. Physicochemical and sorptive properties of biochars derived from woody and herbaceous biomass. *Chemosphere* **2015**, *134*, 257–262. [CrossRef]
9. Vakros, J. Biochars and Their Use as Transesterification Catalysts for Biodiesel Production: A Short Review. *Catalysts* **2018**, *8*, 562. [CrossRef]

10. Shakoob, M.B.; Ali, S.; Rizwan, M.; Abbas, F.; Bibi, I.; Riaz, M.; Khalil, U.; Niazi, N.K.; Rinklebe, J. A review of biochar-based sorbents for separation of heavy metals from water. *Int. J. Phytoremediation* **2019**, *22*, 111–126. [CrossRef] [PubMed]
11. Zabaniotou, A.; Kamaterou, P. Food waste valorization advocating Circular Bioeconomy—A critical review of potentialities and perspectives of spent coffee grounds biorefinery. *J. Clean. Prod.* **2018**, *211*, 1553–1566. [CrossRef]
12. ICO. Annual Review. 2021. Available online: <https://www.ico.org/documents/cy2022-23/annual-review-2021-2022-e.pdf> (accessed on 20 April 2023).
13. Batista, M.J.P.A.; Ávila, A.F.; Franca, A.S.; Oliveira, L.S. Polysaccharide-Rich Fraction of Spent Coffee Grounds as Promising Biomaterial for Films Fabrication. *Carbohydr. Polym.* **2020**, *233*, 115851. [CrossRef] [PubMed]
14. Makri, E.; Tsimogiannis, D.; Dermesonluoglu, E.K.; Taoukisa, P.S. Modeling of Greek coffee aroma loss during storage at different temperatures and water activities. *Procedia Food Sci.* **2011**, *1*, 1111–1117. [CrossRef]
15. Vieira, L.R.; Soares, A.M.V.M.; Freitas, R. Caffeine as a contaminant of concern: A review on concentrations and impacts in marine coastal systems. *Chemosphere* **2021**, *286*, 131675. [CrossRef] [PubMed]
16. FAOSTAT. Available online: <https://www.fao.org> (accessed on 20 April 2023).
17. OIV. Statistical Report on World Vitiviniculture 2019. Available online: <https://www.oiv.int/public/medias/6782/oiv-2019-statistical-report-on-world-vitiviniculture.pdf> (accessed on 20 April 2023).
18. Iuga, M.; Mironeasa, S. Potential of grape byproducts as functional ingredients in baked goods and pasta. *Compr. Rev. Food Sci. Food Saf.* **2020**, *19*, 2473–2505. [CrossRef] [PubMed]
19. Hellenic Statistical Authority (ELSTAT). Available online: [https://www.statistics.gr/documents/20181/18166418/Annual+Agricultural+Statistical+Survey+\(Final+Results\)+\(2020\).pdf/ba0e1942-afaf-12b2-1984-e065f6bd3d72?t=1693558783605](https://www.statistics.gr/documents/20181/18166418/Annual+Agricultural+Statistical+Survey+(Final+Results)+(2020).pdf/ba0e1942-afaf-12b2-1984-e065f6bd3d72?t=1693558783605) (accessed on 27 February 2024).
20. Soufleros, E.H. *Wine and Distillates*; Papageorgiou Pub: Thessaloniki, Greece, 1987.
21. Apostolopoulou, A.A.; Flouros, A.I.; Demertzis, P.G.; Akrida-Demertzi, K. Differences in concentration of principal volatile constituents in traditional Greek distillates. *Food Controls* **2005**, *16*, 157–164. [CrossRef]
22. Soltani, N.; Bahrami, A.; Pech-Canul, M.I.; González, L.A. Review on the physicochemical treatments of rice husk for production of advanced materials. *J. Chem. Eng.* **2015**, *264*, 899–935. [CrossRef]
23. Barana, D.; Salanti, A.; Orlandi, M.; Ali, D.S.; Zoia, L. Biorefinery process for the simultaneous recovery of lignin, hemicelluloses, cellulose nanocrystals and silica from rice husk and *Arundo donax*. *Ind. Crops Prod.* **2016**, *86*, 31–39. [CrossRef]
24. Tala, W.; Chantara, S. Use of spent coffee ground biochar as ambient PAHs sorbent and novel extraction method for GC-MS analysis. *Environ. Sci. Pollut. Res.* **2019**, *26*, 13025–13040. [CrossRef] [PubMed]
25. Jagdale, P.; Ziegler, D.; Rovere, M.; Tulliani, J.M.; Tagliaferro, A. Waste Coffee Ground Biochar: A Material for Humidity Sensors. *Sensors* **2019**, *19*, 801. [CrossRef] [PubMed]
26. Claoston, N.; Samsuri, A.; Husni, M.A.; Amran, M. Effects of pyrolysis temperature on the physicochemical properties of empty fruit bunch and rice husk biochars. *Waste Manag. Res. J. Sustain. Circ. Econ.* **2014**, *32*, 331–339. [CrossRef] [PubMed]
27. Kalaitzidis, S.; Karapanagioti, H.K.; Christanis, K.; Bouzinos, A.; Iliopoulou, E. Evaluation of peat and lignite phenanthrene sorption properties in relation to coal petrography: The impact of inertinite. *Int. J. Coal Geol.* **2006**, *68*, 30–38. [CrossRef]
28. Karapanagioti, H.K.; Sabatini, D.A.; Kleineidam, S.; Grathwohl, P.; Ligouis, B. Phenanthrene sorption with heterogeneous organic matter in a landfill aquifer material. *Phys. Chem. Earth Part B Hydrol. Oceans Atmos.* **1999**, *24*, 535–541. [CrossRef]
29. Sessa, F.; Veeyee, K.F.; Canu, P. Optimization of biochar quality and yield from tropical timber industry wastes. *Waste Manag.* **2021**, *131*, 341–349. [CrossRef] [PubMed]
30. Fuertes, A.B.; Arbertain, M.C.; Sevilla, M.; Maciá-Agulló, J.A.; Fiol, S.; López, R.; Smernik, R.J.; Aitkenhead, W.P.; Arce, F.; Macías, F. Chemical and structural properties of carbonaceous products obtained by pyrolysis and hydrothermal carbonisation of corn stover. *Soil Res.* **2010**, *48*, 618–626. [CrossRef]
31. Cao, X.; Harris, W. Properties of dairy-manure-derived biochar pertinent to its potential use in remediation. *Bioresour. Technol.* **2010**, *101*, 5222–5228. [CrossRef] [PubMed]
32. Zhang, Y.; Ma, Z.; Zhang, Q.; Wang, J.; Ma, Q.; Yang, Y.; Luo, X.; Zhang, W. Comparison of the physicochemical characteristics of bio-char pyrolyzed from moso bamboo and rice husk with different pyrolysis temperatures. *BioResources* **2017**, *12*, 4652–4669. [CrossRef]
33. Yargiloglou, E.N.; Sadasivam, B.Y.; Reddy, K.R.; Spokas, K. Physical and chemical characterization of waste wood derived biochars. *Waste Manag.* **2015**, *36*, 256–268. [CrossRef] [PubMed]
34. Zama, E.F.; Zhu, Y.-G.; Reid, B.J.; Sun, G.-X. The role of biochar properties in influencing the sorption and desorption of Pb(II), Cd(II) and As(III) in aqueous solution. *J. Clean. Prod.* **2017**, *148*, 127–136. [CrossRef]
35. Xu, X.; Zhao, Y.; Sima, J.; Zhao, L.; Mašek, O.; Cao, X. Indispensable role of biochar-inherent mineral constituents in its environmental applications: A review. *Bioresour. Technol.* **2017**, *241*, 887–899. [CrossRef] [PubMed]
36. Dawei, L.; Xiaoxiao, Z.; Yu, W.; Peijie, Z.; Li, Z.; Zongbo, Z.; Xin, G.; Yingyun, Q.; Guixia, L.; Yuanyu, T. Adjusting ash content of char to enhance lithium storage performance of rice husk-based SiO<sub>2</sub>/C. *J. Alloys Compd.* **2020**, *854*, 156986. [CrossRef]
37. Shi, S.-C.; Liu, G.-T. Cellulose nanocrystal extraction from rice straw using a chlorine-free bleaching process. *Cellulose* **2021**, *28*, 6147–6158. [CrossRef] [PubMed]
38. Nikolopoulos, I.; Kordouli, E.; Mourgkogiannis, N.; Karapanagioti, H.K.; Lycourghiotis, A.; Kordulis, C. Valorization of Pyrolyzed Biomass Residues for the Transformation of Waste Cooking Oil into Green Diesel. *Catalysts* **2023**, *13*, 1004. [CrossRef]

39. Kalampaliki, D.; Jayasinghe, G.D.T.M.; Avramiotis, E.; Manariotis, I.D.; Venieri, D.; Pouloupoulos, S.G.; Szpunar, J.; Vakros, J.; Mantzavinos, D. Application of a KOH-activated biochar for the activation of persulfate and the degradation of sulfamethoxazole. *Chem. Eng. Res. Des.* **2023**, *194*, 306–317. [[CrossRef](#)]
40. Kyriakou, M.; Chatziiona, V.K.; Costa, C.N.; Kallis, M.; Koutsokeras, L.; Constantinides, G.; Koutinas, M. Biowaste-based biochar: A new strategy for fermentative bioethanol overproduction via whole-cell immobilization. *Appl. Energy* **2019**, *242*, 480–491. [[CrossRef](#)]
41. Song, B.; Chen, M.; Zhao, L.; Qiu, H.; Cao, X. Physicochemical property and colloidal stability of micron- and nano-particle biochar derived from a variety of feedstock sources. *Sci. Total. Environ.* **2019**, *661*, 685–695. [[CrossRef](#)] [[PubMed](#)]
42. Das, O.; Sarmah, A.K.; Zujovic, Z.; Bhattacharyya, D. Characterisation of waste derived biochar added biocomposites: Chemical and thermal modifications. *Sci. Total. Environ.* **2016**, *550*, 133–142. [[CrossRef](#)] [[PubMed](#)]
43. Burachevskaya, M.; Minkina, T.; Bauer, T.; Lobzenko, I.; Fedorenko, A.; Mazarji, M.; Sushkova, S.; Mandzhieva, S.; Nazarenko, A.; Butova, V.; et al. Fabrication of biochar derived from different types of feedstocks as an efficient adsorbent for soil heavy metal removal. *Sci. Rep.* **2023**, *13*, 2020. [[CrossRef](#)] [[PubMed](#)]
44. Mansaray, K.G.; Ghaly, A.E. Thermal degradation of rice husks in nitrogen atmosphere. *Bioresour. Technol.* **1998**, *65*, 13–20. [[CrossRef](#)]
45. Cantrell, K.B.; Hunt, P.G.; Uchimiya, M.; Novak, J.M.; Ro, K.S. Impact of pyrolysis temperature and manure source on physico-chemical characteristics of biochar. *Bioresour. Technol.* **2012**, *107*, 419–428. [[CrossRef](#)] [[PubMed](#)]
46. Das, S.K.; Ghosh, G.K.; Avasthe, R.K.; Sinha, K. Compositional heterogeneity of different biochar: Effect of pyrolysis temperature and feedstocks. *J. Environ. Manage* **2021**, *278*, 111501. [[CrossRef](#)] [[PubMed](#)]
47. Faghihzadeh, F.; Anaya, N.M.; Schifman, L.A.; Oyanedel-Craver, V. Fourier transform infrared spectroscopy to assess molecular-level changes in microorganisms exposed to nanoparticles. *Nanotechnol. Environ. Eng.* **2016**, *1*, 1–16. [[CrossRef](#)]
48. Usman, A.R.; Abduljabbar, A.; Vithanage, M.; Ok, Y.S.; Ahmad, M.; Ahmad, M.; Elfaki, J.; Abdulazeem, S.S.; Al-Wabel, M.I. Biochar production from date palm waste: Charring temperature induced changes in composition and surface chemistry. *J. Anal. Appl. Pyrolysis* **2015**, *115*, 392–400. [[CrossRef](#)]
49. Fu, P.; Hu, S.; Sun, L.; Xiang, J.; Yang, T.; Zhang, A.; Zhang, J. Structural evolution of maize stalk/char particles during pyrolysis. *Bioresour. Technol.* **2009**, *100*, 4877–4883. [[CrossRef](#)] [[PubMed](#)]
50. Qian, L.; Chen, B. Dual role of biochars as adsorbents for aluminum: The effects of oxygen-containing organic components and the scattering of silicate particles. *Environ. Sci. Technol.* **2013**, *47*, 8759–8768. [[CrossRef](#)] [[PubMed](#)]
51. Mahmud, K.N.; Wen, T.H.; Zakaria, Z.A. Activated carbon and biochar from pineapple waste biomass for the removal of methylene blue. *Environ. Toxicol. Manage.* **2021**, *1*, 30–36. [[CrossRef](#)]
52. Sun, K.; Wang, Y.; Zhang, L.; Shao, Y.; Li, C.; Zhang, S.; Hu, X. High yield of carbonaceous material from biomass via pyrolysis-condensation. *Chem. Eng. J.* **2024**, *485*, 149823. [[CrossRef](#)]
53. Chen, B.; Zhou, D.; Zhu, L. Transitional Adsorption and Partition of Nonpolar and Polar Aromatic Contaminants by Biochars of Pine Needles with Different Pyrolytic Temperatures. *Environ. Sci. Technol.* **2008**, *42*, 5137–5143. [[CrossRef](#)] [[PubMed](#)]
54. Bonelli, P.R.; Della Rocca, P.A.; Cerrella, E.G.; Cukierman, A.L. Effect of pyrolysis temperature on composition, surface properties and thermal degradation rates of Brazil Nut shells. *Bioresour. Technol.* **2001**, *76*, 15–22. [[CrossRef](#)] [[PubMed](#)]
55. Campos, P.; Miller, A.Z.; Knicker, H.; Costa-Pereira, M.F.; Merino, A.; De la Rosa, J.M. Chemical, physical and morphological properties of biochars produced from agricultural residues: Implications for their use as soil amendment. *Waste Manag.* **2020**, *105*, 256–267. [[CrossRef](#)] [[PubMed](#)]
56. Orfanos, A.G.; Manariotis, I.D.; Karapanagioti, H.K. Removal of Methylene Blue from Water by Food Industry By-products and Biochars. *Desalinat. Water Treat.* **2018**, *103*, 113–121. [[CrossRef](#)]
57. Santoso, E.; Ediaty, R.; Kusumawati, Y.; Bahruji, H.; Sulistiono, D.O.; Prasetyoko, D. Review on recent advances of carbon based adsorbent for methylene blue removal from waste water. *Mater. Today Chem.* **2020**, *16*, 100233. [[CrossRef](#)]
58. Thommes, M.; Kaneko, K.; Neimark, A.V.; Olivier, J.P.; Rodriguez-Reinoso, F.; Rouquerol, J.; Sing, K.S.W. Physisorption of gases, with special reference to the evaluation of surface area and pore size distribution (IUPAC Technical Report). *Pure Appl. Chem.* **2015**, *87*, 1051–1069. [[CrossRef](#)]

**Disclaimer/Publisher’s Note:** The statements, opinions and data contained in all publications are solely those of the individual author(s) and contributor(s) and not of MDPI and/or the editor(s). MDPI and/or the editor(s) disclaim responsibility for any injury to people or property resulting from any ideas, methods, instructions or products referred to in the content.